Journal of Catalysis **201,** 236–246 (2001)
doi:10.1006/jcat.2001.3246, available online at http://www.idealibrary.com on IDEAL®

Morphology and Surface Properties of Boehmite (γ-AlOOH): A Density Functional Theory Study

P. Raybaud,* M. Digne,* R. Iftimie,* W. Wellens,* P. Euzen,† and H. Toulhoat*

*Division Chimie et Physico-Chimie Appliquées; and †Division Cinétique et Catalyse Institut Français du Pétrole, 1–4 avenue de Bois-Préau, 92852 Rueil-Malmaison Cedex, France

Received January 9, 2001; revised March 28, 2001; accepted March 28, 2001

The aluminum oxihydroxide boehmite (γ-AlOOH) is the topotactic precursor of γ-alumina, widely used as a support of refining catalysts. We use ab initio calculations and molecular dynamics (MD) to study water–boehmite interfacial properties, which are believed to play a key role during the industrial synthesis of boehmite in aqueous solution. For four relevant crystallographic planes—(010), (100), (001), and (101)—we develop a theoretical approach for calculating surface energies and interfacial energies that cannot be determined experimentally. From these values, the morphology of boehmite nanosized particles is constructed either in vacuum or in water, highlighting the strong effect of the solvent. It is clearly shown that during MD water molecules react on the surfaces by molecular adsorption and dissociative chemisorption, producing surface hydroxyl groups. A detailed analysis of the local structure before and after water adsorption is furnished. Particularly, four main surface hydroxyl groups are identified by their stretching vibrational frequencies: μ_2-Al$_{VI}$ ($\nu_{OH} = 3676$ cm^{-1}), μ_1-Al$_{VI}$ ($\nu_{OH} = 3712$ cm^{-1}), μ_1-Al$_V$ ($\nu_{OH} = 3741$ cm^{-1}), and μ_1-Al$_{IV}$ ($\nu_{OH} = 3819$ cm^{-1}). This analysis of surface hydroxyl groups gives us some new insights for the understanding of experimental IR band assignment and Brønsted acidity by ammonia adsorption. The localization of basic and acid Brønsted sites on the boehmite nanosized particles is resolved. An interpretation of these results in the light of γ-alumina is attempted.

Key Words: **boehmite; γ-alumina; DFT calculations; molecular dynamics; interfacial properties; surface energy; morphology; Brønsted acidity; infrared analysis; hydroxyl group; vibrational frequencies.**

I. INTRODUCTION

Boehmite, or aluminum oxihydroxide (γ-AlOOH), is the precursor of the most important of industrial catalysts supports: γ-alumina (γ-Al_2O_3). γ-Al_2O_3 plays an important role in industry, widely used as a catalyst carrier (1, 2) in refining (3, 4) such as reforming (5, 6), isomerization (7), hydrotreatment (8), and hydroconversion of residues (9). This is the reason why the surface properties of γ-Al_2O_3 have been the subject of extensive experimental investigations for many years. In particular, Brønsted acidity can be characterized by infrared (IR) spectroscopy of the surface hydroxyl groups. Nevertheless, IR analysis encountered difficulties in assigning unambiguously the great number of observed OH stretching vibrational frequencies within the range 3650 to 3800 cm^{-1} to the right types of surface hydroxyl groups (10–14). Although several models have been proposed in the literature (10–13) to identify the IR vibrational frequencies, some controversy still exists (15, 16).

At the same time, few experimental studies (17, 18) on the surface properties of boehmite have been reported, although the hydroxide precursor is at the core of the industrial preparation of the resulting support. Upon controlled calcination under air flow, boehmite undergoes a topotactic transformation into γ-Al_2O_3 so that the conserved morphology and size of boehmite nanosized particles are reflected in those of the final transition alumina. All important textural properties of the industrial catalysts (surface area, pore size distribution, pore shapes, etc.) are essentially determined at the boehmite production step. A recent ab initio study (19) of the γ-AlOOH to γ-Al_2O_3 transformation underlines the fundamental role of the precursor on the inherited bulk properties of the final support. Furthermore, the interactions between boehmite particles occurring at the peptizing step are governed by surface properties. Many factors such as pH, temperature, and aqueous mother solution composition influence the solid/liquid interfacial energies, which in turn determine the size and morphologies of boehmite crystallites (2, 20, 21). It is well known however that solid/liquid interfacial energies are not directly accessible experimentally, but at best their ratios can be deduced from the observation of experimental morphologies (21–23). Another center of interest is found in adding catalytic active phase precursors at the boehmite stage (24). In this case, the surface properties of boehmite should be described precisely since it governs the interactions with active phase precursors.

In an effort to develop a well-founded prediction of these effects of obvious industrial outcomes, we propose first in the present paper a strategy for evaluating ab initio

0021-9517/01 $35.00

interfacial energies for the water–boehmite interface. The Gibbs–Curie–Wulff law enables determination of the morphology of boehmite nanocrystallites in a region of pH close to the zero point charge (ZPC) according to our simulations. Then, we calculate ab initio stretching vibrational frequencies of surface hydroxyl groups and adsorption enthalpies of ammonia to characterize Brønsted acidity of the nanocrystallites with the well-defined morphology. These results will be compared with experimental data on this system (17, 18). We are convinced that this approach also brings new insights and helpful arguments for a better understanding of IR experimental results obtained on γ-Al_2O_3 as far as the Brønsted acid sites simulated on boehmite within this work can be regarded as relevant models for γ-alumina.

II. METHODS

A. Bases of DFT Calculations

Our calculations are based on density-functional theory, using the local exchange-correlation functional proposed by Perdew and Zunger (25), corrected for nonlocal effects by using the generalized gradient corrections developed by Perdew *et al.* (26). Electronic eigenstates are expanded in terms of plane waves, using ultrasoft pseudopotentials (27, 28) to describe the electron–ion interactions. The solution of the generalized Kohn–Sham equations valid for a system modeled by ultrasoft pseudopotentials is performed using the Vienna Ab-Initio Simulation Package (VASP) (28–30). VASP performs an iterative diagonalization of the Kohn–Sham Hamiltonian via unconstrained band-by-band minimization of the norm of the residual vector to each eigenstate and optimized charge density mixing routines. The optimization of the atomic geometry at 0 K is performed by using a conjugate gradient algorithm and by determining the exact Hellman–Feynman forces acting on the ions determined at each optimization step. A Verlet algorithm is used for integrating Newton's equations of motion during molecular dynamics (MD). For the aluminum atom, the atomic reference configuration is $3s^2 3p^1$ and for the oxygen atom, $2s^2 2p^4$. The calculations have been performed using the soft oxygen potential and thus a relatively small energy cutoff of 300 eV. Hydrogen has also been modeled by an ultrasoft pseudopotential for an atomic reference of $1s^1 1p^0$.

We have carried out MD in the (NVT) ensemble by equilibrating the temperature of the system using a Nosé thermostat procedure (31). The temperature of the simulation is 350 K and corresponds to the usual experimental conditions of boehmite preparation. The MD time step is 0.5 fs after replacing hydrogen by the deuterium atom. The total MD duration as reported in Table 1 depends on the iteration number before reaching equilibration, given by the stabilization of the internal energy of the system.

TABLE 1

Parameters Used for the Simulation of the Bulk Phase, the Water Layer, and the Interface Systems

	Bulk	010	100	001	101
Number of atoms	16	96(+36)[a]	96(+36)	80(+36)	64(+36)
Slab thickness (Å)	—	18.0	9.2	9.3	9.1
Surface areas (Å^2)	—	43.0	87.5	69.1	56.2
Surface periodicity	—	$2\vec{a} \times 2\vec{c}$	$1\vec{b} \times 2\vec{c}$	$2\vec{a} \times 1\vec{b}$	$1\vec{u} \times 1\vec{b}$
K-point mesh	844	411	111	211	211
Water thickness (Å)	—	8.4	4.0	5.3	6.6
Total MD-time (ps)	1.1	0.5	1.5	1.1	1.5

[a] Corresponding to 12 water molecules.

B. Morphology Determination

The interfacial energy for the $\langle hkl \rangle$ orientation, Γ_{hkl}, is given by the equation

$$\Gamma_{hkl} = \frac{G_{hkl} - G_{bulk} - G_{water}}{2 \cdot S_{hkl}}, \qquad [1]$$

where G_{hkl} is the free energy of the oriented water–boehmite interface (its average value is calculated at $T =$ 350 K over the last 0.5 ps once the equilibration is reached), G_{bulk} is the reference free energy of the bulk phase of boehmite containing the same number of atoms as in the slab and at $T = 350$ K, G_{water} is the reference free energy of the liquid water at $T = 350$ K, and S_{hkl} stands for the area of the oriented surface.

For surface energies calculated in vacuum, Eq. [1] can be simplified by the relationship

$$\Gamma^{vac}_{hkl} = \frac{G^{vac}_{hkl} - G_{bulk}}{2 \cdot S_{hkl}}, \qquad [2]$$

where G^{vac}_{hkl} is the free energy of the boehmite surface in vacuum including relaxation effects at $T = 0$ K. Later on in the paper, $\Gamma^{vac^*}_{hkl}$ will stand for the surface energy in vacuum without relaxation.

When the entropic contributions are neglected, the free energies, G, will be approximated by the internal energy of the system, E. So the notation E will be preferred in what follows.

The morphologies derived by this approach will correspond to equilibrium morphologies since boehmite particles produced experimentally (21) and of industrial interest exhibit characteristic sizes of a few nanometers or even smaller. The formula [2] differs slightly from the one proposed by Gay *et al.* (32) since in our case we are dealing with supercells containing slabs simulating the oriented surfaces instead of semi-infinite models. The slab thickness is large enough to mimic bulk properties for atoms located close to the center of the slab (see Fig. 3a) and to ensure that

both sides are independent. Hence, the surface energy is deduced by subtracting the energy reference of a bulk supercell (and water supercell) from the total energy of the slab for the same composition.

For a fixed volume of the boehmite crystallite and at thermodynamic equilibrium, the Gibbs–Curie–Wulff law enables construction of the morphology by applying the relationship

$$\frac{\Gamma_{hkl}}{d_{hkl}} = A; \quad \forall\, h,k,l, \qquad [3]$$

where d_{hkl} is the distance from the surface to the center of mass of the solid, and A a real number independent of h,k,l.

Equation [3] is equivalent to minimizing the total interfacial energy, E_{tot},

$$E_{tot} = \sum_{hkl} S_{hkl}\Gamma_{hkl}, \qquad [4]$$

with the constraint that the total volume,

$$V_{tot} = \frac{1}{3}\sum_{hkl} S_{hkl}d_{hkl}, \qquad [5]$$

is held fixed.

C. Vibrational Frequency Mode of Hydroxyl Groups

We calculate ab initio OH vibrational stretching modes in vacuum for the different hydroxyl groups formed after MD simulation, considering that according to the experimental procedures (17, 18) all physisorbed molecules are removed after heating at 423 K in vacuum. We assume that this mode is a pure one uncoupled from the rest of the motion of the boehmite structure. So we have performed this calculation assuming the rest of the boehmite structure as fixed. Due to the small mass of hydrogen, the quantum behavior of this atom should be taken into account. We follow the procedure proposed by Ugliengo *et al.* (33) and successfully applied for characterizing the Brønsted acidity of zeolite systems (34, 35). The potential energy is calculated for each value of the OH distance around the equilibrium position and is fitted by a sixth-order polynomial within the interval [−0.3 Å, + 0.4 Å]. The lowest vibrational levels are calculated by solving the one-dimensional nuclear Schrödinger equation (36) as implemented in the ANHARM program (37).

The anharmonicity constants $\omega_e\chi_e$ are estimated from the frequencies of the two lowest eigenmodes,

$$2\omega_e\chi_e = 2\omega_{01} - \omega_{02}, \qquad [6]$$

and the corresponding harmonic frequencies are given by the following relation:

$$\omega_e = \omega_{01} + 2\omega_e\chi_e. \qquad [7]$$

All notations that have been defined within this section are used in the following paragraphs of the paper.

III. RESULTS AND DISCUSSION

A. Boehmite Bulk

The bulk structure of boehmite has been studied extensively in the past by X-Ray Diffraction (XRD) (38–41), Infra-Red (IR) spectroscopy (42–46) and Nuclear Magnetic Resonance (NMR) (47). Boehmite exhibits a lamellar structure within an orthorhombic symmetry (Fig. 1). Each layer constitutes the (OAlOH–HOAlO) stacking sequence in the x- and z-direction. The octahedral aluminums are surrounded by four tetrahedral oxygens and two hydroxyl groups. The cohesion of the stacked layers in the y-direction is ensured by hydrogen bonds between hydroxyl groups belonging to two consecutive layers and forming a zig-zag chain along the z-direction.

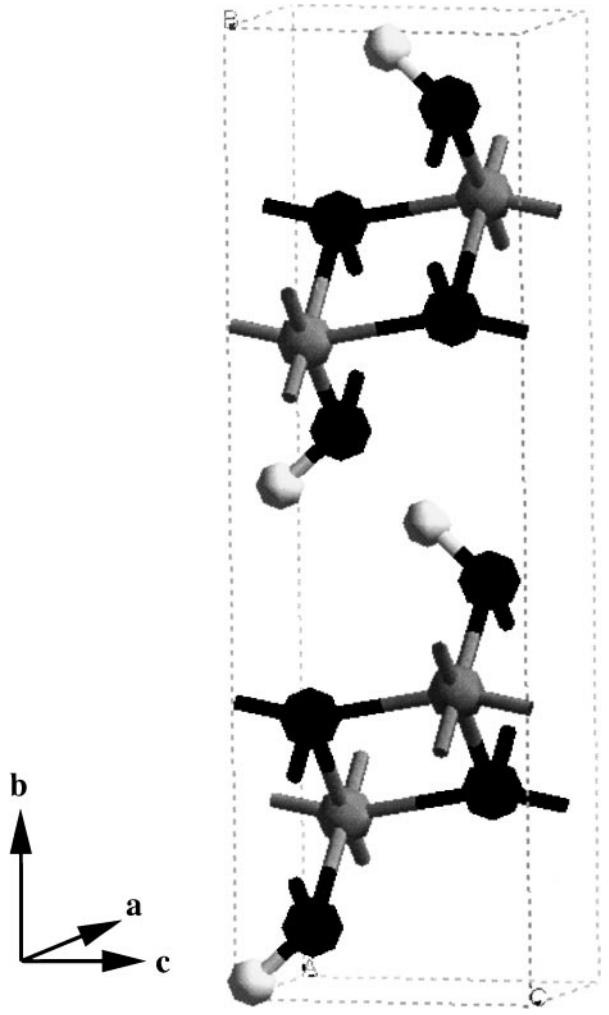

FIG. 1. Unit cell of the boehmite bulk containing 4 AlOOH units. Black balls: oxygen atoms; gray balls: aluminum atoms; white balls: hydrogen atoms.

TABLE 2

Energetics of the Differently Oriented Surfaces in Vacuum and of the Corresponding Boehmite–Water Interfaces

hkl	Γ_{hkl}^{vac*} (mJ · m^{-2})	Γ_{hkl}^{vac} (mJ · m^{-2})	Area^{vac} %	E_{hkl} (eV/cell)	E_{water} (eV/cell)	Γ_{hkl} (mJ · m^{-2})	Area %
010	455	455	61	−799.08	−174.53	465	44
100	2630	1860	15	−794.91	−175.07	650	22
001	1980	1165	24	−691.34	−175.26	750	20
101	4585	3000[a]	0	−586.56	−174.41	825	14

Note. Surface areas and interfacial areas correspond to morphologies displayed in Fig. 7.
[a] Approximate value.

The optimized parameters for the bulk phase, $a = 2.90$ Å, $b = 11.97$ Å, $c = 3.71$ Å, and $V = 128.63$ Å^3, are in rather good agreement with the experimental parameters (41): $a_{exp} = 2.87$ Å, $b_{exp} = 12.23$ Å, $c_{exp} = 3.69$ Å, and $V_{exp} = 129.63$ Å^3. The slight underestimation of the b parameter due to the difficulty in describing hydrogen chemical bond strength within DFT formalism will have only a minor effect on the surface energetics and surface properties that involve mainly Al–O and O–H iono-covalent bond breaking or formation.

The mean internal energy, E_{bulk}, after MD simulation at $T = 350$ K is equal to −104.51 eV per cell containing four AlOOH units.

B. Energetics of Surfaces and Reactivity

We have chosen the (010), (100), (001), and (101) planes as the most relevant crystallographic orientations.

The oriented interfacial energies are plotted in Fig. 2 as a function of time using Eq. [1] with the mean values of the internal energies of the bulk phase, E_{bulk}, and of the water cell, E_{water}.

The surface energies, Γ_{hkl}^{vac}, calculated in vacuum, the internal energies E_{hkl} of the interfaces, and the interfacial energies, Γ_{hkl}, calculated at the end of the equilibration in water are reported in Table 2.

To simulate the corresponding interfacial systems, we use a thin water layer to separate the neighboring slab of boehmite. According to periodic boundary conditions, the water layer is sandwiched between the boehmite's slabs. Figures 3a, 4a, 5a, and 6a represent the supercells containing the ideally as-cleaved oriented slabs in vacuum and without relaxation. The same boehmite slab is used for relaxations done in vacuum and for MD in the presence of water. All relevant slabs parameters are reported in Table 1, such as the size of slabs (thickness of water or vacuum). In particular, it has been checked carefully that the thickness of each slab and the thickness of the vacuum are sufficient in ensuring that each side of the slab behaves as an independent interface.

The surface areas of the oriented planes, S_{hkl}, (used in Eqs. [1] and [2]) are given in Table 1 and represented in Figs. 3–6 by dotted planes. This choice of relative large surface areas is justified by the fact that surfaces exhibiting multiple periodicities with respect to the bulk periodicity allow reconstructions as well as adsorptions of multiple water molecules on unequivalent surface sites. Furthermore, the minimal k-point number required to describe the first Brillouin zone has been tested. Indeed, it is of first importance to ensure the k-point convergence to calculate interfacial energies with sufficient accuracies.

The water layer contains 12 water molecules within a volume corresponding to a density of 0.9 at $T = 350$ K. According to the relative small size of the water box, its internal energy, E_{water}, depends also slightly on the orientation. To be consistent, we have considered different reference energies for the liquid phase according to the orientation (Table 2). Nevertheless, this deviation remains significantly smaller than the final relevant differences obtained on the interfacial energies. Starting from the ionic positions of the ideally as-cleaved surface and water layer, we allow the water-surface to react chemically by performing MD at $T = 350$ K. Once the internal energy of the water–boehmite system converges, we check for the saturation of adsorption at the interface by eventually "re-filling" the interslab liquid space to compensate for the consumption of water by reaction at the interface.

(010) surface. In Fig. 2, we observe first that the (010) surface reaches equilibration the most rapidly (after 0.15 ps), characterizing very weak interfacial relaxation effects. At the end of the equilibration, this surface exhibits the smallest interfacial energy. The surface energy in vacuum at 0 K and the interfacial energy in water at $T = 350$ K are very close: 455 and 465 mJ m^{-2}, respectively. The generation of this surface implies that only 31.2 μmol m^{-2} of hydrogen bonds are cut (Table 3). This corresponds to 14.6 kJ mol^{-1} of hydrogen bond, which is in gross agreement with experimental knowledge. This explains why the surface energy is the lowest in vacuum and why the chemical reactivity remains weak in water: water molecules are only physisorbed on this surface.

(100) and (001) surfaces. The (100) and (001) surfaces exhibit intermediate behaviors. Indeed, their surface energies in vacuum and interfacial energies in vacuum range

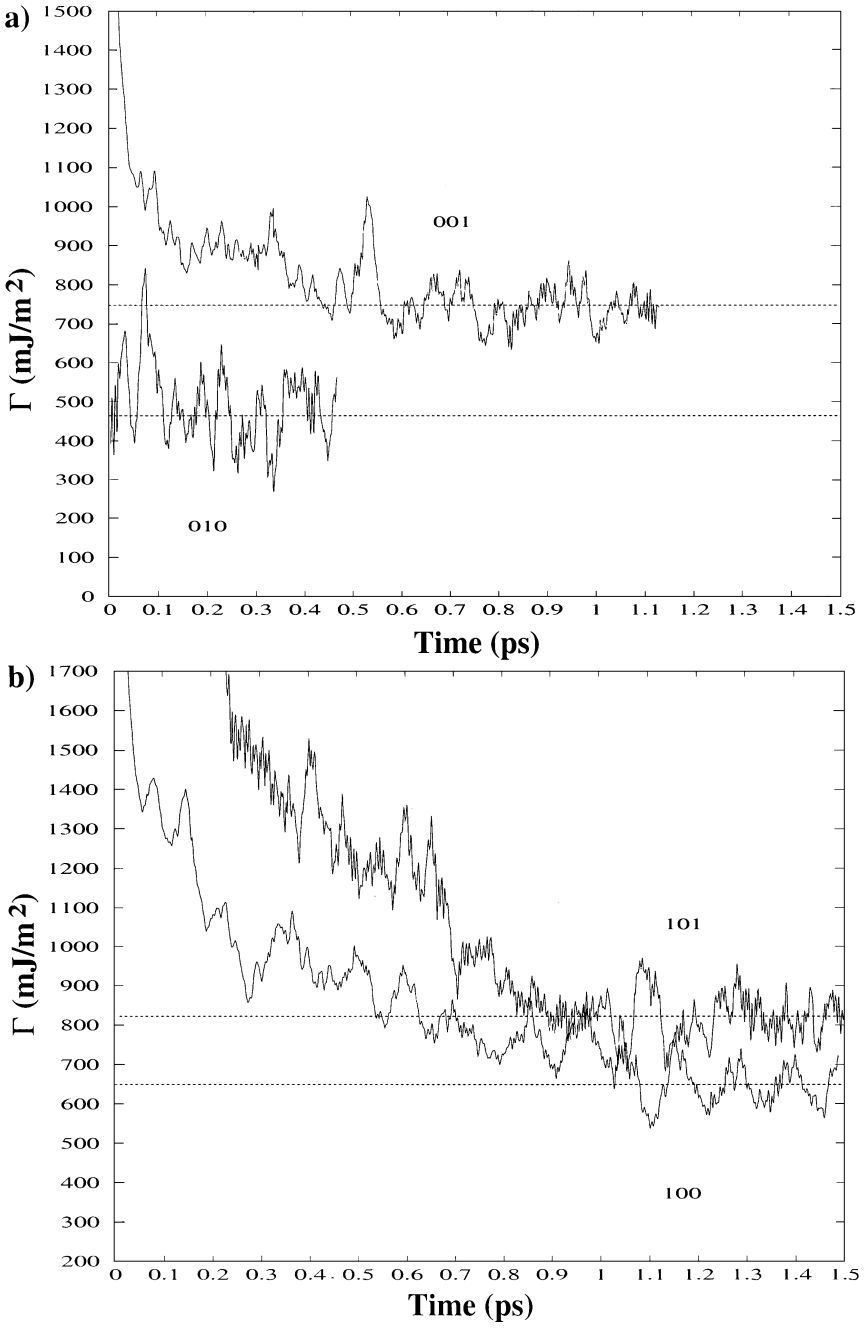

FIG. 2. Variation of the interfacial energies (in $mJ \cdot m^{-2}$) as a function of time (in ps) during the molecular dynamics of water–boehmite systems.

between the values of the (010) and (101) orientations: 1860 and 1165 mJ m^{-2}, respectively, corresponding to 29.4 and 18.9 μmol m^{-2} of Al–O bonds cut. For the (100) surface the Al–O bond energy is about 90 kJ mol^{-1} while for the (001) orientations it is 104 kJ mol^{-1}. Furthermore, it is interesting to observe that the order of magnitude of surface energies are comparable to those obtained in vacuum on corundum (α-Al_2O_3) (32). We confirm simultaneously that relaxation effects modify significantly the surface energies and hence cannot be neglected. The equilibration times are about 1.0 and 0.6 ps for the (100) and (001) interfaces, respectively. This means that their reactivities with the solvent are also intermediate with a higher reactivity than exhibited by the (001) interface. The interfacial energies are in a reverse order in comparison with the surface energies, due to the higher reactivity of the (100) orientation. So the effect of the environment will be critical for determining the morphology.

TABLE 3

Coordination Numbers of Surface Aluminum Atoms, N_{Al}, and of Oxygen Atoms, N_O, and Numbers of Al–O Bonds or of Hydrogen Bonds Per Surface Area, Initially Cut, N_{bonds}

	010		100		001		101	
Surface	Initial	Final	Initial	Final	Initial	Final	Initial	Final
N_{Al}	6	6	4	5–6	5	5–6	3	4
N_O	3–4	3–4	2–3	2–4	3	3–4	2	2–3
N_{bonds} (μmol · m^{-2})	31.2	—	29.4	—	18.9	—	34.8	

(101) surface. For the (101) surface, the equilibration time is the longest: about 1.0 ps is required. The surface energy in vacuum without relaxation is the highest: 4585 mJ m^{-2}. The effects of surface relaxation in vacuum are huge and the relaxed surface energy is estimated to be about 3000 mJ m^{-2}. This is explained by the fact that the number of Al–O bonds cut, 34.8 μmol m^{-2}, is also the highest and corresponds to 131 kJ mol^{-1} of Al–O bond. At the end of the MD equilibration in water, the interfacial energy is 825 mJ m^{-2} and remains the highest, although it has been significantly decreased by water stabilization.

Finally, in vacuum, surface energy values vary within 455 mJ m^{-2} and at least 1860 mJ m^{-2}, whereas in water this range of variation diminishes strongly between 465 and 825 mJ m^{-2}. This result demonstrates that the solvent effect of water tends to level surface energies. This will have of course a direct influence on the morphology.

C. Morphology and Local Structure

Morphology analysis. From the energetics, the morphology of a nanosized boehmite crystallite can be determined using the Gibbs–Curie–Wulff law as described in the Computational section. It should be underlined that the simulation in water corresponds to zero point charge (ZPC) only since no charged species are introduced on the surface or in water.

We have constructed the morphology in two cases: in vacuum (Fig. 7a) and in water (Fig. 7b). It is obvious that the observed morphology depends strongly on the environment. In particular, the percentages of the (010) surface areas (Table 2) varies between 61% (in vacuum) and 44% (in water). In both cases, this surface, also called the basal surface, represents the major area, while the other surfaces are the edge surfaces of the nanocrystallite. The solvent tends to stabilize the edge surfaces (100), (101), and (001) versus the basal one by adsorbing water on their aluminum unsaturated sites as explained in the following section.

Among the edge surfaces, the (101) surface is one of the most strongly stabilized by water and its percentage is about 14% in water whereas in vacuum this surface does not exist. The proportion of the (100) and (001) surfaces remains rather similar either in vacuum or in water, although there is a slight inversion of their area percentages (Table 2).

(010) surface. On the basal (010) surface (Fig. 3), all the aluminum sites and oxygen atoms are fully saturated since the ideal as-cleaved surface implies that only hydrogen bonds are cut. From energetics as well as from structural analysis, this surface is highly unreactive and exhibits a local environment in water very similar to the one obtained in vacuum (Table 3). Each aluminum atom is bound to two bridging hydroxyl groups: these OH species will be refered as the μ_2-Al$_{VI}$ types.

(100) surface. In vacuum, the ideal as-cleaved (100) surfaces exhibits four-fold-coordinated aluminum atoms bound to two oxygen atoms three-fold-coordinated (Table 3). The surface reconstruction in vacuum implies the formation of a corrugated surface due to the outward relaxations of the three-fold-coordinated oxygen atoms (Fig. 4b). This leads to an ondulated chain of Al–O–Al–O where oxygen atoms are two-fold-coordinated and aluminium atoms are in a perfect tetrahedral environment. The water adsorption on the unsaturated aluminium atoms prevents this outward relaxation of oxygen atoms (Fig. 4c). After MD equilibration, the average number of coordination of surface aluminum is increased to a value of 5 or 6. Simultaneously, a great number of surface OH groups has been created (Fig. 4c) via dissociative adsorption of water molecules according to the following mechanism:

$$Al\text{–}\square + Al\text{–}O\text{–}\square + H_2O \rightarrow 2Al\text{–}OH. \qquad [8]$$

This produces two main types of surface hydroxyl groups: the μ_1-Al$_{VI}$ and μ_1-Al$_V$ types. Some nondissociated water molecules remain also adsorbed.

(001) surface. On the (001) surface, all aluminium atoms are initially five-fold-coordinated in an octahedral environment, while oxygen atoms are threefold-coordinated (Table 3 and Fig. 5a). After relaxation in vacuum, we observe in Fig. 5b that there is an inward relaxation

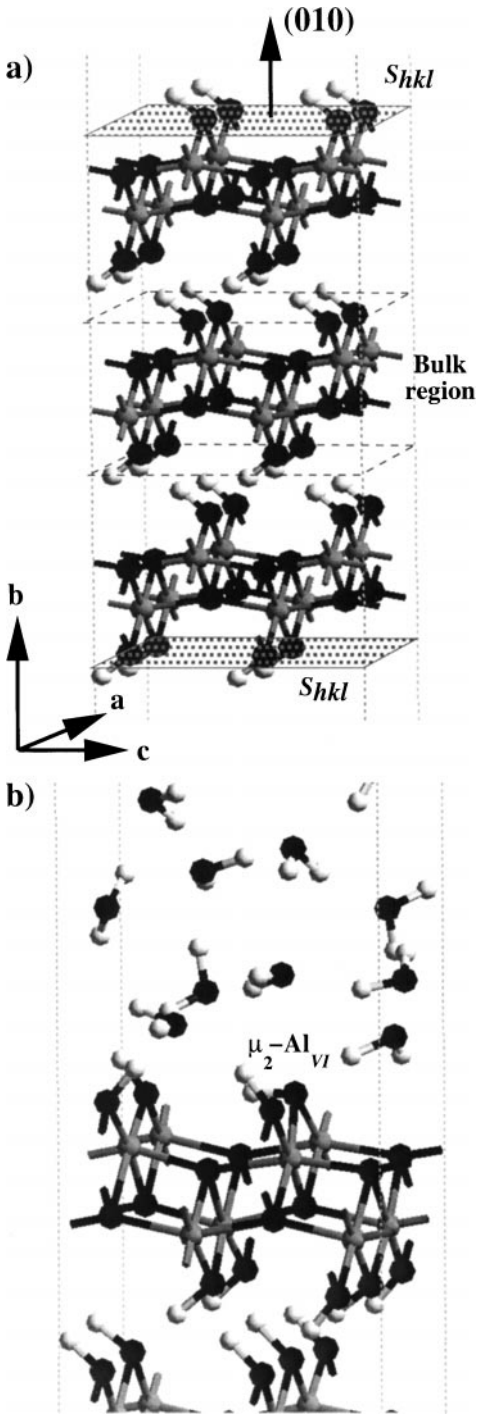

FIG. 3. (a) Relaxed configuration in vacuum at 0 K of the as-cleaved (010) surface; (b) configuration equilibrated at $T = 350$ K of the water–boehmite (010) interface. The planes represented by dotted areas stand for the S_{hkl} surfaces on each side of the slab. (Same legend as Fig. 1.)

of aluminum atoms. Such structural changes in vacuum are well known for other types of oxides (48, 49). Unlike the (100) surface for which the chemical adsorption of water governs the interfacial stabilization, on the (001), there is a competition between water adsorption and the inward relaxation of the surface aluminium atoms. This explains why a significant number of Al surface sites remain five-fold-coordinated and can be regarded as weak Lewis acid sites. Furthermore, when a water molecule adsorbs on such an aluminum site, it induces an outward relaxation of the aluminum atom (Fig. 5c), leading to a distorted octahedral environment of aluminum. The hydroxyl groups formed are considered μ_1-Al$_V$ types.

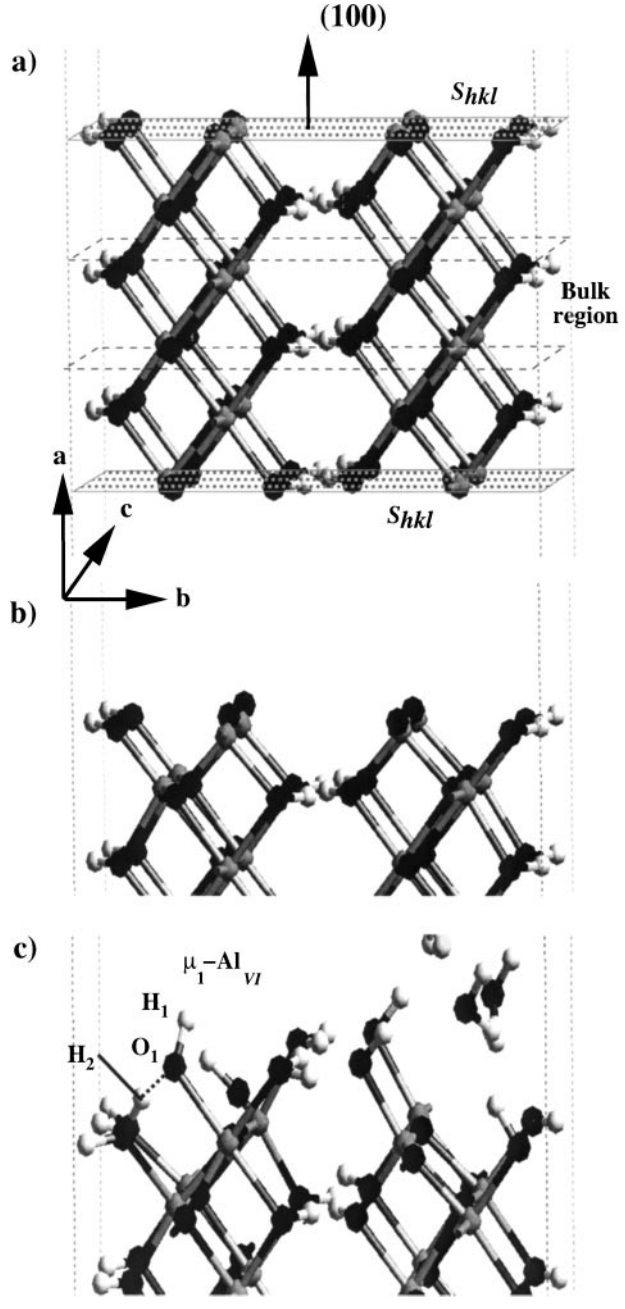

FIG. 4. (a) Initial configuration of the as-cleaved (100) surface; (b) relaxed configuration in vacuum at 0 K; (c) configuration equilibrated at $T = 350$ K of the water–boehmite (100) interface. (Same legend as Fig. 1.)

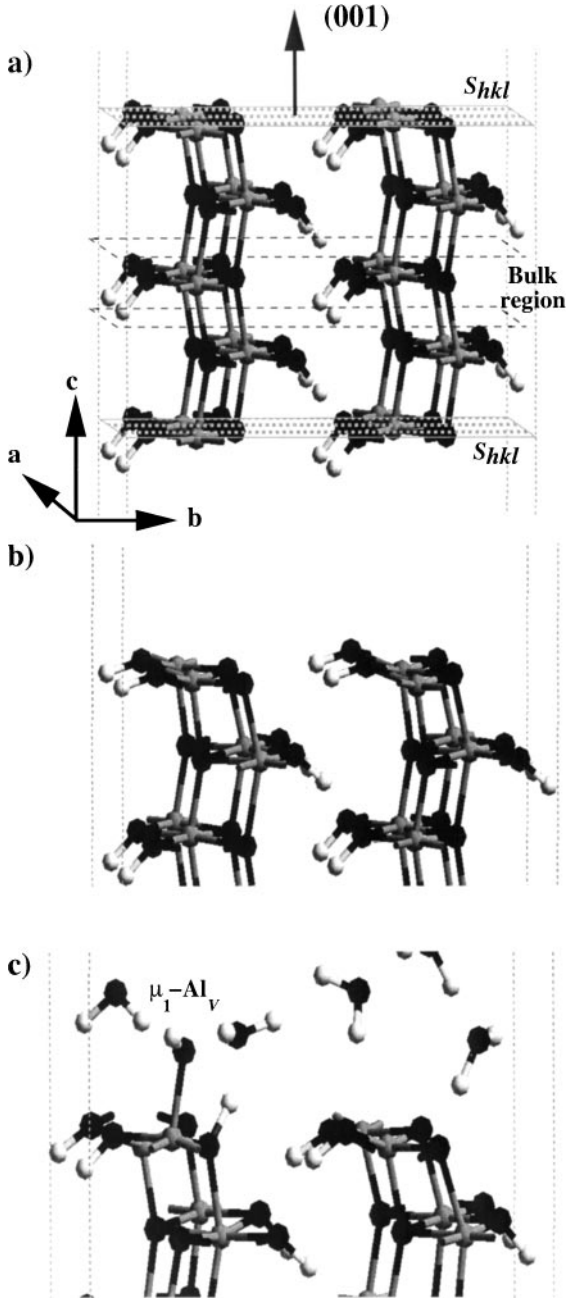

FIG. 5. (a) Initial configuration of the as-cleaved (001) surface; (b) relaxed configuration in vacuum at 0 K; (c) configuration equilibrated at $T = 350$ K of the water–boehmite (001) interface. (Same legend as Fig. 1.)

(101) surface. The (101) as-cleaved surface exhibits two kinds of surface aluminium sites: the fully saturated aluminum sites with bridging oxygen atoms and threefold aluminum atoms (Table 3 and Fig. 6). In the presence of water, a great number of chemical reactions occur following a similar mechanism as [8] and forming exclusively surface hydroxyl groups from the μ_2-Al$_{VI}$ and μ_1-Al$_{IV}$ types (Fig. 6b).

D. Hydroxyl Stretching Mode Analysis and Brønsted Acidity

In the previous section, we analyzed the different local environments of four oriented surfaces, revealing the presence of four possible hydroxyl groups: μ_2-Al$_{VI}$, μ_1-Al$_{VI}$, μ_1-Al$_V$, and μ_1-Al$_{IV}$. According to the morphology predicted previously, the fraction of each type of site on the boehmite crystallite in an aqueous environment can be estimated and is reported in Table 4. It shows clearly that μ_2-Al$_{VI}$ groups are present in the majority at 75% (including the (010) and (101) surfaces), followed by the μ_1-Al$_{VI}$ groups representing 12% of the OH sites and located on the (100) surface. The least frequent OH groups are the μ_1-Al$_V$ and μ_1-Al$_{IV}$ ones with 5 and 8%, respectively.

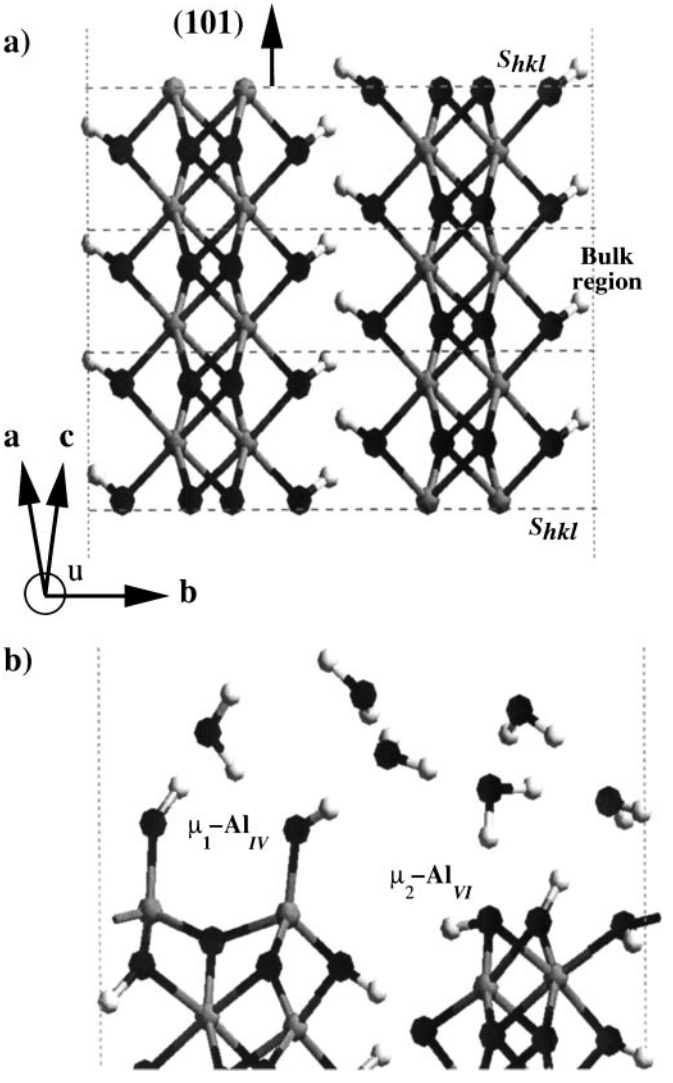

FIG. 6. (a) Relaxed configuration in vacuum at 0 K of the as-cleaved (101) surface; (b) configuration equilibrated at $T = 350$ K of the water–boehmite (101) interface. (Same legend as Fig. 1.)

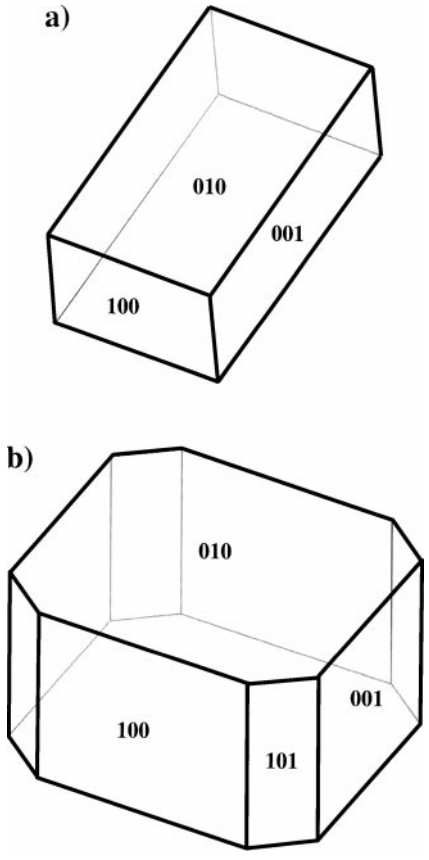

FIG. 7. Nanonosized boehmite crystallite morphologies calculated by injecting the energetics as reported in Table 2 into the Gibbs–Curie–Wulff law (see Text): (a) in vacuum, (b) in water.

The stretching modes of the different OH groups have been calculated so as to mimic the experimental procedures (17, 18) where all physisorbed molecules are evaporated after heating at 423 K in vacuum. So after MD simulation all remaining water molecules corresponding to physisorbed states have been removed for the vibrational analysis. The results are reported in Table 4 including the corresponding local Al–O and O–H distances. It should be noticed that, for μ_1-Al type groups, the vibrational frequencies of stretching modes correlates well with the O–H length: the higher the ν_{OH}, the smaller the O–H distance.

From the IR experiments (17, 18), the boehmite spectra exhibit two bands corresponding to the internal hydroxyl groups at 3088 and 3287 cm^{-1}. These are discussed in detail in the literature (42–46) and are beyond the scope of our work. A well-controlled heating process implying desorption of a physisorbed water molecule as described in (18) enables the revealing of two other bands in the region of surface hydroxyl groups at about 3665–3668 cm^{-1} with a rather high intensity and 3695–3705 cm^{-1} with a significantly smaller intensity (17, 18). According to our results, we find that the most frequent μ_2-Al_{VI} groups present on the (010) basal surface (and for a minor fraction on the (101) surface) vibrate at 3676 cm^{-1}. So we assign the experimental band at about 3665–3668 cm^{-1} with the highest intensity to the surface μ_2-Al_{VI} hydroxyl groups (with an eventual contribution of the OH of the (101) surface). We propose that the second IR band, located at 3695–3705 m^{-1}, contains as a main contribution the μ_1-Al_{VI} types for which the calculated stretching frequency is at 3712 cm^{-1}. An eventual contribution of the μ_1-Al_V group at 3741 cm^{-1} cannot be fully excluded.

We have also calculated the stretching mode of the μ_1-Al_{IV} hydroxyl groups revealed by our simulations on the (101) surface. The frequency modes are at 3810 cm^{-1} but should lead to a minor contribution since they represent only 8%. None of the available experimental IR studies report these vibrational frequencies on boehmite. This can be due to experimental conditions for preparing the boehmite sample, leading to a slightly different morphology, implying a smaller amount of the (101) surface than the one calculated in pure water at zero point charge within our work.

As a consequence of the four different models for surface hydroxyl groups, the ranking of the vibrational values for the stretching modes is as follows: μ_1-Al_{IV} > μ_1Al_V > μ_1-Al_{VI} > μ_2-Al_{VI}. It shows clearly that the OH stretching frequencies are influenced by the coordination number of oxygen: μ_1-Al_{VI} > μ_2-Al_{VI} (see also Refs. (12, 16, 49)). However, our results demonstrates clearly that it depends also on the coordination number of the aluminum atoms to which the hydroxyl groups are bonded: μ_1-Al_{IV} > μ_1-Al_V > μ_1-Al_{VI}.

TABLE 4

Local Structure (All Distances are in Å) and Vibrational Stretching Frequencies (in cm^{-1}) of Surface Hydroxyl Groups

Type (surface)	Proportion (%)	d(OH)	d(AlO)	ω_{01}	ω_{02}	ω_e	$\omega_e\chi_e$
μ_2-Al_{VI} (010)	67	0.990	1.904–1.908	3676	7200	3826	75
μ_2-Al_{VI} (101)	8	0.991	1.889–1.976	3691	7221	3852	81
μ_1-Al_{VI} (100)	12	0.990	1.832	3712	7271	3865	77
μ_1-Al_V (001)	5	0.988	1.755	3741	7325	3897	78
μ_1-Al_{IV} (101)	8	0.980	1.659	3819	7479	3977	79

Note. See Methods for the definitions of ω and χ.

TABLE 5

Local Structure and Adsorption Enthalpies of NH_3 on Three Brønsted Sites and One Water Site

Site	d(NH) (Å)	d(HO) (Å)	ΔH (kJ · mol^{-1})
OH–μ_1–Al_V	1.948	1.005	−34.3
OH–μ_1–Al_{IV}	1.705	1.017	−55.5
OH–μ_2–Al_{VI}	1.724	1.031	−61.5
H_2O–μ_1–Al_{VI}	1.598	1.053	−86.1

Although we are well aware of the differences between the surface properties of boehmite and those of γ-Al_2O_3, it is interesting to compare this result with the IR assignment proposed for γ-Al_2O_3. The three species simulated previously can be regarded as models for the OH groups encountered on γ-Al_2O_3 surfaces. The ranking obtained previously would correspond for γ-Al_2O_3 to the following one: $I_a > I_b > II$ using Knözinger's notation (12), for which I_a stands for μ_1-Al_{IV}, I_b for μ_1-Al_{VI}, and II for μ_2-Al_{VI}. So the highest frequencies observed at about 3800 cm^{-1} on γ-Al_2O_3 would actually be assigned to type I_a groups. This assignment would be in favor of Morterra's (14) and Busca's (15) proposals.

Finally, we have calculated the adsorption enthalpies at 0 K of a basic model molecule, NH_3, to investigate the acid strength of previously defined relevant Brønsted sites. The results obtained after a full optimization of the geometry are reported in Table 5. The O–H distances of the hydroxyl groups and the N–H distances at equilibrium are reported. The larger the O–H distance, the more advanced the protonic transfer and the more favorable the adsorption energy. The ranking of the adsorption enthalpies is as follows: μ_1-$Al_V > \mu_1$-$Al_{IV} > \mu_2$-Al_{VI}. This confirms clearly that the hydroxyl groups of the basal plane exhibit the highest acid strength whereas the edge planes (101), (001), and (100) contain mainly the basic hydroxyl groups. The adsorption enthalpies on the water molecules is even stronger, which characterizes an even stronger acid group. The adsorption enthalpy of NH_3 on the O_1H_1–μ_1-Al_{VI} (Fig. 4c) site is about −42.6 kJ mol^{-1}, a surprisingly low value according to the general assumption that the μ_1-Al_{VI} group should be more basic than the μ_1-Al_V group. Nevertheless, according to the local structure of the site, we are able to put forward that a cooperative effect of two neighboring OH groups can take place during the adsorption of NH_3. Indeed, the full relaxation of the system leads to the transfer of one hydrogen atom, H_2, coming from the neighboring OH_2 group to the oxygen atom, O_1, of the hydroxyl group where NH_3 adsorbs (see Fig. 4c). This implies a stabilization of the adsorbed NH_3. For γ-alumina, this phenomenon can play a significant role and depends directly on the hydroxylation state of the surface (13).

As a corollary of fundamental interest for catalysis, our study shows clearly that the strongest Brønsted acid sites of boehmite are located on the (010) basal plane, while the basic ones are on the edge planes.

IV. CONCLUSION

In this paper we presented calculations based on the density-functional theory (DFT) and applied it to detailed investigations on aluminum oxihydroxide, boehmite, precursor of the catalytic carrier γ-alumina. We have proposed an approach to determine morphologies of the vacuum–boehmite and water–boehmite sytems using ab initio molecular dynamics for precise calculations of surface energies and interfacial energies in water.

This makes it possible to demonstrate first the significant effect of the solvent on the modification of the morphologies and so on the surface properties of boehmite. In vacuum, the surface energies are directly correlated to the number of Al–O bonds or hydrogen bonds, which are cut after generating the as-cleaved surface. In water, crystallographic planes exhibiting high surface energies in vacuum are stabilized due to water molecules adsorption. Different chemical mechanisms have been revealed during MD such as water physisorption, water molecular chemisorption, and dissociative chemisorption. The latter chemical event explains the formation of surface hydroxyl groups during the preparation of the boehmite sample.

In agreement with experimental IR analysis, we have proposed an assignment of the observed surface hydroxyl groups by calculating their vibrational stretching modes. For the different surface hydroxyl groups of boehmite, the following ranking of the stretching frequencies is found: μ_1-$Al_{IV} > \mu_1$-$Al_V > \mu_1$-$Al_{VI} > \mu_2$-Al_{VI}. A Brønsted acidity scale has been established by calculating NH_3 adsorption enthalpies. This analysis has enabled us to locate the strongest Brønsted acid sites of boehmite nanosized particles on the basal surface, while the basic centers are on the edge plane.

Finally, we attempted to give an interpretation of our results considering the γ-alumina system discussed in detail in the literature. If the surface hydroxyl groups simulated on boehmite can be regarded as relevant for some surface species of γ-alumina surfaces, our assignment would converge with Busca's or Morterra's. Nevertheless, we remain cautious since it is well known that, unlike boehmite, the spinel-like structure of γ-alumina contains vacancies underlying the surface hydroxyl groups. The precise effects of these vacancies on the OH surface stretching frequencies and on the Brønsted acidity are not well understood. We hope to be able to investigate further this issue in the near future by simulating realistic models of γ-Al_2O_3 surfaces.

ACKNOWLEDGMENTS

We thank our colleagues G. Mabilon from the Institut Français du Pétrole (France) as well as Prof. J.-P. Jolivet and C. Froidefond from the

Université Pierre et Marie Curie (France) for the numerous scientific exchanges. We are grateful to Prof. J. Hafner, Prof. G. Kresse, and Th. Demuth from the Universität Wien (Austria) for very fruitful scientific discussions. We are indebted to J. Ángyán from the Université de Nancy (France) and Y. Jeanvoine from the Université d'Evry (France) for making available the ANHARM program.

REFERENCES

1. Oberlander, K., *in* "Applied Industrial Catalysis" (B. E. Leach, Ed.), Vol. 3, pp. 63–112. Academic Press, NewYork, 1984.
2. Poisson, R., Nortier, P., and Brunelle, J. P., *in* "Catalysts and Supported Catalysts" (A. B. Stiles, Ed.), pp. 11–55. Butterworths, Boston, 1987.
3. Lepage, J. F., *in* "Applied Heterogeneous Catalysis." pp. 75–123. Technip Ed., Paris, 1987.
4. Martino, G., Courty, P., and Marcilly, C., *in* "Handbook of Heterogeneous Catalysis" (G. Ertl, H. Knözinger, and J. Weitkamp, Eds.), pp. 1802–1818. VCH Verlag Gesellschaft, Weinheim, Germany, 1997.
5. Gates, B. C., Katzer, J. R., and Schuit, G. C. A., *in* "Chemistry of Catalytic Process," Chem. Eng. Ser., pp. 92–150. McGraw-Hill, New York, 1992.
6. Gilsdorf, N., *in* "Encyclopedia of Chemical Processing and Design" (J. J. McKetta, Ed.), Vol. 47, pp. 92–150. Dekker, New York, 1992.
7. Trombetta, M., Busca, G., Rossini, S., Picolli, V., Cornaro, U., and Guercio, A., Catalani, R., and Willey, R. J., *J. Catal.* **179**, 581 (1998).
8. Stork, W. H. J., *in* "Hydrotreatment and Hydrocracking of Oil Fractions" (G. F. Froment, B. Delmon, and P. Grange, Eds.), pp. 41–67. Elsevier, Amsterdam, The Netherlands, 1997.
9. Morel, F., Kressmann, S., Harlé, V., and Kasztelan, S., *in* "Hydrotreatment and Hydrocracking of Oil Fractions" (G. F. Froment, B. Delmon, and P. Grange, Eds.), pp. 1–16. Elsevier, Amsterdam, The Netherlands, 1997.
10. Peri, J. B., *J. Phys. Chem.* **69**, 220 (1965).
11. Tsyganenko, A. A., and Filimonov, V. N., *Spectrosc. Lett.* **5**, 477 (1972); Tsyganenko, A. A., and Filimonov, V. N., *J. Mol. Struct.* **19**, 579 (1973).
12. Knözinger, H., and Ratnasamy, P., *Catal. Rev.-Sci. Eng.* **17**(1), 31 (1978).
13. Tsyganenko, A. A., and Mardilovitch, P. P., *J. Chem. Soc. Faraday Trans.* **92**, 4283 (1996).
14. Morterra, C., Ghiotti, G., Garrone, E., and Boccuzzi, F., *J. Chem. Soc. Faraday Trans. 1* **72**, 2722 (1976).
15. Busca, G., Lorenzelli, V., Sanchez Escribano, V., and Guidetti, R., *J. Catal.* **131**, 167 (1991).
16. Morterra, C., and Magnacca, G., *Catal. Today* **27**, 497 (1996).
17. Lewis, D. G., and Farmer, V. C., *Clay Miner.* **21**, 93 (1986).
18. Morterra, C., Emanuel, C., Cerrato, G., and Magnacca, G., *J. Chem. Soc. Faraday Trans.* **88**(3), 339 (1992).
19. Krokidis, X., Raybaud, P., Gobichon, A. E., Rebours, B., Euzen, P., and Toulhoat, H., *J. Phys. Chem. B*, in press.
20. Vayssières, L., Ph.D. thesis. Université Pierre et Marie Curie, Paris, 1995.
21. Froidefond, C., Ph.D. thesis. Université Pierre et Marie Curie, Paris, 2001.
22. Lin, Z., and Ward, M. D., *Analytical Chem.* **68**, 1285 (1996).
23. Balkenende, A. R., Van de Boogaard, H. J., Scholten, M., and Willard, N. D., *Langmuir* **14**, 5907 (1998).
24. Van Veen, J. A. R., Hendriks, P. A. J. M., Romers, E. J. G. M., and Andreéa, R. R., *J. Phys. Chem.* **94**, 5275 (1990).
25. Perdew, J. P., and Zunger, A., *Phys. Rev. B* **23**, 5084 (1987).
26. Perdew, J. P., Chevary, J. A., Vosko, S. H., Jackson, K. A., Pedersen, M. R., Singh, D. J., and Frolhais, C., *Phys. Rev. B* **46**, 6671 (1992).
27. Vanderbilt, D., *Phys. Rev. B* **41**, 7892 (1990).
28. Kresse, G., and Hafner, J., *Phys. Rev. B* **47**, 588 (1994); ibid. **49**, 14251 (1994).
29. Kresse, G., and Hafner, J., *J. Phys. Condens. Matter* **6**, 8245 (1994).
30. Kresse, G., and Furthmüller, J., *Comput. Mater. Sci.* **6**, 15 (1996); ibid. *Phys. Rev. B* **54**, 11961 (1996).
31. Nosé, S., *Prog. Theor. Phys. Suppl.* **103**, 1 (1991).
32. Gay, D. H., and Rohl, A. L., *J. Chem. Soc. Faraday Trans.* **91**(5), 925 (1995).
33. Senchenya, I. N., Garrone, E., and Ugliengo, P., *J. THEOCHEM* **368**, 93 (1996).
34. Jeanvoine, Y., Àngyàn, J. G., Kresse, G., and Hafner, J., *J. Phys. Chem. B* **102**, 5573 (1998).
35. Demuth, Th., Hafner, J., Benco, L., and Toulhoat, H., *J. Phys. Chem. B* **104** (19), 4593 (2000).
36. Lindberg, B., *J. Chem. Phys.* **88**(6), 3805 (1988).
37. Ugliengo, P., ANHARM—A program to solve numerically the monodimensional nuclear Schrödinger equation. Unpublished.
38. Farkas, L., Gadó, P., and Werner, P. E., *Mater. Res. Bull.* **12**, 1213 (1977).
39. Tettenhorst, R., and Hofmann, D. A., *Clays Clay Miner.* **28**, 373 (1980).
40. Hill, R., *Clays Clay Miner.* **29**, 435 (1981).
41. Corbató, C. E., Tettenhorst, R. T., and Cristoph, G. G., *Clays Clay Miner.* **33**(1), 71 (1985).
42. Wickersheim, K. A., and Korpi, G. P., *J. Chem. Phys.* **42**(2), 579 (1965).
43. Fripiat, J. J., Bosmans, H., and Rouxhet, P. G., *J. Phys. Chem.* **71**, 1097 (1967).
44. Russel, J. D., and Farmer, V. C., *Spectrochim. Acta B* **34**, 1151 (1978).
45. Kiss, A. B., Keresztury, G., and Farkas, L., *Spectrochim. Acta A* **36**, 653 (1979).
46. Farmer, V. C., *Spectrochim. Acta A* **46**, 585 (1979).
47. Slade, R. C. T., and Halstead, T. K., *J. Solid State Chem.* **32**, 119 (1980).
48. Manissidis, I., De Vita, A., and Gillan, M. J., *Surf. Sci.* **295**, L517 (1993).
49. Haas, K. C., Schneider, W. F., Curioni, A., and Andreoni, W., *J. Phys. Chem. B* **104**, 5527 (2000).